ACS OMEGA

http://pubs.acs.org/journal/acsodf

Article

Power Generation by a Double-Sided Tape

Moon-Hyung Jang, Jacob D. Lee, Yu Lei, Simon Chung, and Gang Wang*

Cite This: *ACS Omega* 2022, 7, 42359−42369

Read Online

ACCESS | Metrics & More | Article Recommendations | Supporting Information

ABSTRACT: A novel contact−separation triboelectric generator concept is proposed in this study, which is composed of a double-sided tape with acrylic adhesive material and a metalized polyester (PET/Al) film (an aluminum layer coating on one side). The proposed concept is very cost-effective and easy to fabricate compared to existing triboelectric nanogenerators (TENGs), which require special equipment and sophisticated procedure to build. The strong bonding nature of acrylic adhesive on the tape induces a significant charge when contacting. The peak power generation depends on the induced pressure at the impact. During the separation phase, the air breakdown between triboelectric layers allows most existing electrons to flow back from the ground due to rapid charge removal at the interface. A higher voltage can be generated when the PET is interfaced with the double-sided tape compared to the Al-acrylic configuration because of the effect of triboelectric series and a Schottky barrier formation for electrons at the tape−Al interface during contact. A double-electrode configuration with an assembly of Al/PET−tape−PET/Al significantly improved the performance, in which a 21.2 mW peak power is achieved compared to 7.6 mW in the single-electrode design with tape−PET/Al assembly when excited at 20 Hz in a shaker test. This double-electrode triboelectric generator can power 476 LEDs with an active area of 38 mm × 25 mm. Moreover, a direct power of a 650 nm laser diode was demonstrated. In summary, the proposed triboelectric generator concept using tacky materials shows the potential for higher-energy harvesting via triboelectrification and advances the state of the art by offering low cost and easy fabrication options. It is expected that such newly proposed triboelectric generators are able to meet power requirements in many engineering applications.

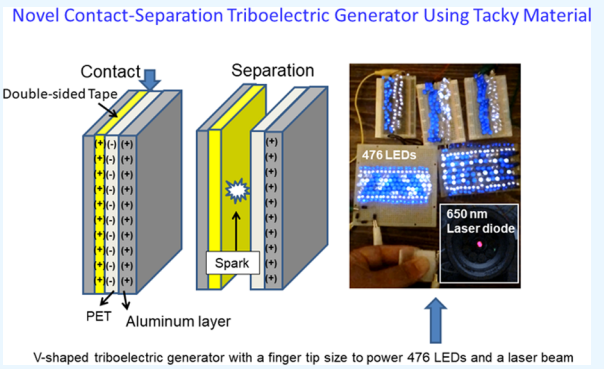

INTRODUCTION

Various adhesives have been developed for thousands of years using animal parts, natural rubbers, and recently synthetic materials to bond different objects. From the late 19th and the early 20th centuries, adhesive tapes, which contain adhesive-coated backing materials, have been introduced. Today, adhesive tapes are one of the essential items for everyday life. In the 21st century, these tapes, specifically pressure-sensitive tapes, which can bond when pressure is applied, have been used in various applications. Nobel Prizes in physics were given to Andre Geim and Konstantin Novoselov for "groundbreaking experiments regarding the two-dimensional material graphene."[1] Common pressure-sensitive tapes were used for separating a graphene layer from bulk graphite in their research. Researchers from UCLA were able to generate X-rays by unrolling pressure-sensitive tapes *in vacuo*, which is called "triboluminescence."[2] Accelerated electrons generate Brems-strahlung X-rays when they strike the positive side of the tape during tape unrolling. The intensity of the X-ray was enough to take a radiogram of a human finger. In this paper, we will show that pressure-sensitive tapes can also be utilized to generate electricity using the triboelectric phenomenon as small-scale energy harvesters. Electrical power generation by a small-scale energy harvesting device is needed to power low-power profile electronic systems in many different applications.[3−12] These include structural health monitoring, wearable sensors, and environmental monitoring systems. To minimize the environmental impact, these should be built as stand-alone systems with the capability of harvesting ambient mechanical energy and converting it into electrical power. Triboelectricity, defined as generating power by electrostatic charges through a friction of two surfaces with different materials, has been introduced for being used as an energy harvesting device. Since its invention in 2012, the triboelectric nanogenerator (TENG) is one of the most promising candidates for small-scale energy harvesters.[8,9,13,14] This process allows converting mechanical energy into electrical energy using the triboelectric effect and electrostatic charges. Triboelectric layers can be selected from the various combination of materials from the triboelectric series to maximize the power generation. For example, Cu and poly(tetrafluoroethylene) (PTFE: Teflon) combination/poly-

Received: August 24, 2022
Accepted: October 26, 2022
Published: November 8, 2022

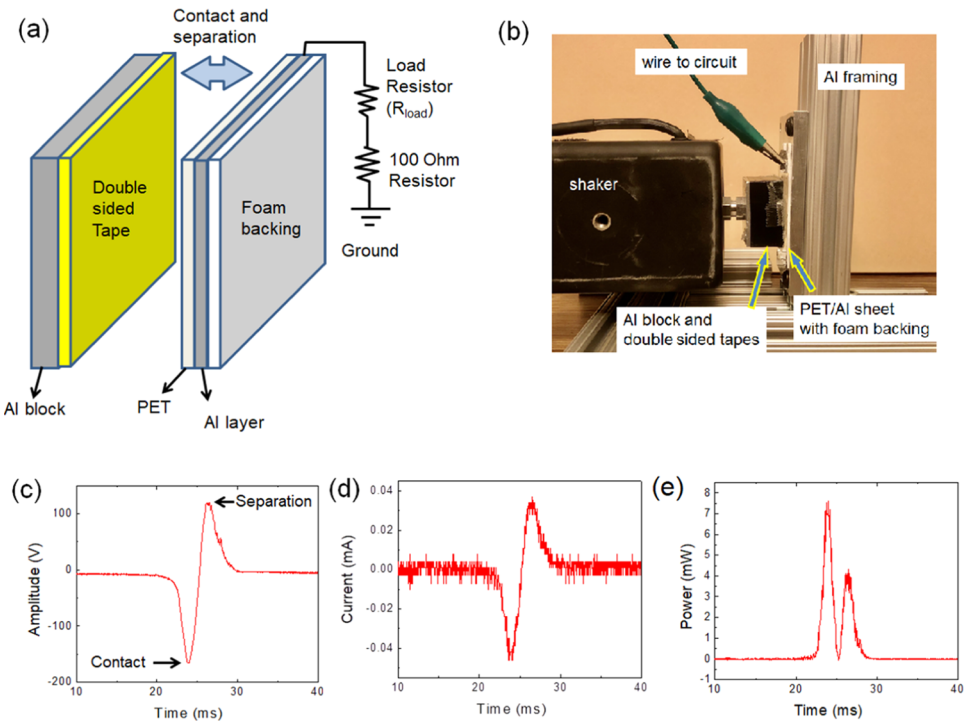

Figure 1. (a) Schematic for the contact−separation triboelectric generator with double-sided tape and Al/PET sheet. (b) A picture of the actual triboelectric generator configuration with a modal shaker. (c) Voltage amplitude and (d) current values as a function of time during the contact−separation process. Negative and positive amplitudes are detected in contact and separation processes, respectively. (e) Power output as a function of time during the contact−separation process.

(methyl methacrylate) (PMMA) and polyimide combination can be used for positive and negative triboelectric layers.[15,16] Those combinations can generate electrical currents by touching each other like contact−separation and sliding. Previously, researchers have developed TENGs with many different modifications such as circuitry designs, different triboelectric materials, different methods of contacting, and different atmospheres. The improvement of TENG performance has been conducted in this way to increase the charge density to achieve higher power density. For example, instead of a normal direction contact−separation, the sliding of triboelectric layers is also commonly used to generate electricity.[17] Even though there have been many significant improvements in the performance of TENGs, to design and build a TENG is complicated. Therefore, it is very costly to integrate TENG in real applications due to the sophisticated structure layout, circuitry optimization, and fabrication scheme.[8,9,13] One challenge is mostly avoiding the air breakdown problem between two triboelectric layers. For example, researchers fabricated a main TENG device with a charge excitation TENG.[16] Moreover, voltage multiplying circuits (VMCs) with Zenor diode were used to boost and stabilize the output voltage.[18] With this design, the maximum current density of 1.25 mC/m^2 and the maximum power density of 38.2 W/m^2 were obtained at a load resistance of 4 MΩ and a frequency of 4 Hz. The charge density of 2.20 mC/m^2 and the power density of 40 W/m^2 are achieved using a ferroelectric P(VDF-TrFE) layer and a VMC circuit.[18] Even though the excitation TENG was no longer used, the ferroelectric layer needs to be integrated into the design with all of the different layers. VMC is still required for the TENG system. Recently, the highest power density of a TENG at 115.6 W/m^2 with an external charge excitation module to avoid the air breakdown between triboelectric layers was established with a carbon/silicone gel electrode in the contact−separation TENG.[19] Therefore, the design of contact−separation-based TENGs shows a high complexity for harvesting electrical power from environmental sources. Moreover, the fabrication process for a complete TENG system is preferred to not give a large environmental impact by avoiding the chemical and evaporation processes.

To advance the development of TENG devices in various engineering applications, we need to address two major challenges,[20] which include the enhancement of power density in triboelectric series and the simplification of fabrication. Detailed quantification on the triboelectric properties of a wide range of materials was conducted to serve as a standard for implementing the application of triboelectrification for energy harvesting.[21,22] One could build a TENG device by exploring those material candidates. However, the fabrication difficulties involved in creating microstructures or special patterns on the surface of selected triboelectric materials, the selection of special equipment, and carefully designed fabrication scheme as observed in the typical TENG device development make this difficult for practical uses.

In this paper, a novel triboelectric generator concept is proposed, in which a simple design was adopted by using a conventional double-sided tape (with acrylic adhesive layer) and a metalized polyester film (i.e., an aluminum layer coating on one side) (PET/Al) to serve as triboelectric layers. It is worth noting that no special fabrication scheme is required in the current design. Power generation is achieved via a contact−separation motion, as shown in a similar TENG device. During the contact phase, the proposed triboelectric generator behaves similarly as observed in a typical contact−separation TENG device, in which charges are developed on the interface

https://doi.org/10.1021/acsomega.2c05457
ACS Omega 2022, 7, 42359−42369

between a double-sided tape and a PET/Al layer. However, the strong bonding nature of acrylic adhesive on the tape induces a significant charge compared to that of a non-tacky triboelectric layer. During the separation phase, the air breakdown via an electric spark occurs at the interface. Such rapid charge removal in triboelectric layers allows existing electrons from the ground flow back to the aluminum layer to realize a different mechanism compared to the capacitance behavior, as observed in a typical TENG device. The tackiness in the adhesive layer contributes to the improved energy generation during the contact and separation phase in the current design. Output power also depends on the induced pressure during the impact in a contact−separation motion. It has better efficiency for contacting PET to a tape surface compared to contacting Al to a tape surface because of the effect of triboelectric series as well as a Schottky barrier formation at the aluminum interface. Both single-electrode and double-electrode designs were investigated. A single-electrode design involves a double-sided tape and a PET/Al layer, in which the aluminum side is served as one electrode along with a ground connection. A double-electrode design leads to a three-layered configuration in which a double-sided tape layer is sandwiched between two PET/Al sheets and both aluminum sides serve as electrode connections. Comprehensive shaker tests from 15 to 25 Hz were conducted to evaluate the performance of the proposed triboelectric generators with double-sided tape materials. We are able to obtain a 21.2 mW peak power in a double-electrode design and 7.6 mW in a single-electrode design, respectively, in which the excitation frequency is at 20 Hz.

Using this double-electrode system, a number of different manually operated generator prototypes were designed and developed, including a spring load prototype, which produced 169.6 W/m^2 while operating approximately at 2 Hz, and a V-shaped prototype, which was capable of powering 476 LEDs with an active area of 38 mm × 25 mm. Moreover, we are able to directly power a 650 nm laser diode using the double-electrode triboelectric generator driven by a shaker at 20 Hz.

In summary, the first contact−separation triboelectric generator was proposed, prototyped, and evaluated by exploring tacky materials as a triboelectric layer. Comparable performance is achieved in our simple design using double-sided tape material.

METHODS

A commercial off-the-shelf (COTS) Pen + Gear double-sided tape was selected to work as one triboelectric layer. Another triboelectric layer was a metallized PET film (PET/Al) from McMaster-Carr with a 50.8 μm thickness, in which an aluminum layer is coated on one side. A Fourier transform infrared (FTIR) spectrum measurement was performed for the tape using a Nicolet IR100 FTIR (Thermo Fisher Scientific), as shown in Figure S1. The spectrum matches well with the feature of a typical acrylic adhesive.[23] A shaker test was performed to evaluate the proposed triboelectric generator, as shown in Figure 1a,b.

A double-sided tape was attached to an aluminum block connected to a shaker head (Smart Shaker 2007E01 from The Modal Shop, Inc.). To realize a contact−separation motion, the tape/Al block assembly was driven at a frequency range from 15 to 25 Hz to impact the PET/Al film, which is attached to an Al fixture, as shown in Figure 1a,b. The initial gap was set at 2 mm. The contact area has a size of 35 mm by 35 mm. A force sensor 208C01 (PCB Piezotronics) was used between the shaker head and the AL block to record the force/pressure measurements during the contact−separation motion. Electrical wirings from the Al layer to the circuit were configured with regular alligator clips. For the power measurement, a 1008A 8-channel USB digital oscilloscope (Hantek) was used. As shown in Figure 1a, a 100 Ω resistor was introduced in the circuit. Its voltage signals (denoted by $V_{circuit}$) were recorded using a digital oscilloscope. Then, the current values (denoted by $I_{circuit}$) in this series circuit were obtained by Ohm's law ($I_{circuit} = I_{100\Omega} = V_{100\Omega}/100\ \Omega$). Finally, the available harvested power can be derived by calculating the product of $V_{circuit}$ and $I_{circuit}$. Note that the typical open circuit voltage (V_{OC}) and short circuit current (I_{SC}) are measured to compute harvested power. This method does not reflect the actual power generation, and it has a tendency of being extraordinarily high (e.g., 133.6 mW at 70 MΩ in our system). Voltage amplitude values of the load resistor and the 100 Ω resistor were measured in channels 1 and 2, as shown in Figure 1a. Channel 3 was used for a force sensor. Channels 4 and 5 were used for voltage and current measurements for another PET/Al sheet for a double-electrode configuration in which additional PET/Al is introduced, as shown in Figure 5a for a double-electrode configuration.

To demonstrate the performance of our single-electrode triboelectric generator, a total of 476 LEDs were lit using a bridge rectifier built with four FR207 diodes. Further improvement was conducted for our triboelectric generator by introducing a double-electrode configuration, i.e., Al/PET−tape−PET/Al assembly. Both shaker and manual contact and separation tests were carried out to evaluate its performance. Substantial improvement in power generation is observed using this double-electrode design, in which a 21.2 mW peak power is achieved compared to 7.6 mW in the single-electrode configuration when excited at 20 Hz in a shaker test. Moreover, we are able to directly power a 650 nm laser diode and record it using a DET100A2 photodetector with a 320−1100 nm spectral range (Thorlabs, Inc.). Endurance test was performed to investigate the effectiveness of the adhesive layer in a shaker test, in which 100,000 contact and separation cycles are achieved. SEM images of PET and double-sided tape layer were included to examine the surface morphology before and after the test, which are measured by a Zeiss LEO 1550 field-emission SEM system at a beam energy of 1 keV with a 112 μA beam current.

RESULTS AND DISCUSSION

Figure 1c,d shows the voltage and the current time history under 20 Hz excitation during a shaker test, in which a 4 MΩ load resistor is used because it shows the optimum power generation, as described in the later part of the paper. Interestingly, the voltage signal shows a large negative value of −166.17 V during the contact phase. Different polarity of voltage amplitude is observed in the separation phase, and its peak amplitude is 122.67 V. Compared to the existing contact/separation TENGs in the literature, the opposite polarity of voltage occurs instantaneously at the initiation of separation. In those studies, it was shown that such positive voltage occurs at a later stage with almost a half-cycle delay.[16,19] However, as shown in Figure S2, our generator shows amplitude inversion at the moment between the contact and separation. This strongly indicates that rather than the field-induced charge movement as observed in triboelectric layers, charges in our system instantly interact during the operation.[24] It will be

https://doi.org/10.1021/acsomega.2c05457
ACS Omega 2022, 7, 42359−42369

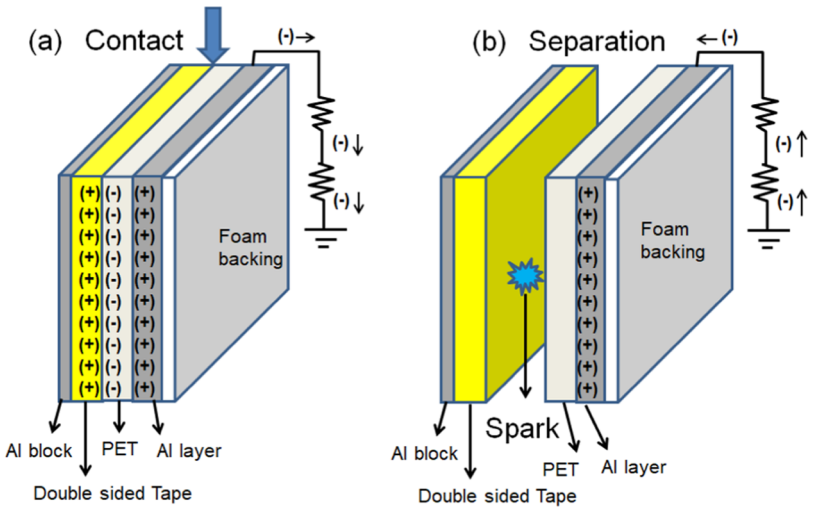

Figure 2. Schematics of a triboelectric generator. (a) In contact, the charge generation occurs at the interface between the double-sided tape and PET layer. (b) In separation, because the double-sided tape and PET will give an electric spark, almost all negative charges are gone in the PET layer. The remaining positive charges in Al will be compensated by electrons from the ground.

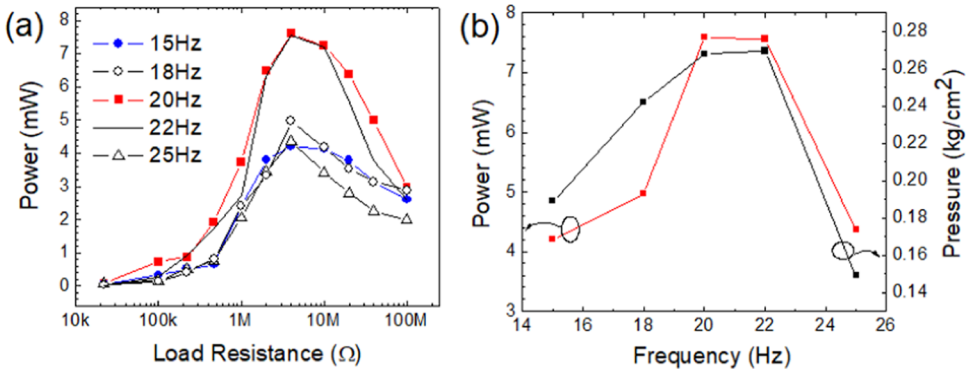

Figure 3. (a) Power generation with different load resistances at different frequencies from 15 to 25 Hz. Since the natural frequency of the system is between 20 and 22 Hz, higher peak power generation occurs at this frequency range. (b) Comparison of peak power generation and applied pressure for triboelectric generator as a function of frequency. In the natural frequency range of system, the applied pressure increases as resonance occurs so that the generation of power increases significantly.

explained in the later part of this paper. The amount of power, which is a product of voltage and current, was plotted as a function of time, as shown in Figure 1e. As aforementioned, our power calculation was obtained by multiplying the measured voltage from a 100 Ω resistor, and the peak value is 7.6 mW. The corresponding power density is 6.2 W/m^2 by assuming a 35 mm × 35 mm contact area. Impressively, our current triboelectric design with a double-sided tape and a PET/Al sheet achieves a comparable power density to existing TENGs in the literature. Note that the charge interaction plays a crucial role in our simple triboelectric generator design. Figure 2a shows the charge development during the contact phase. Similar to existing TENGs, a formation of an electrical double layer occurs at the interface between two triboelectric layers. Accordingly, the double-sided tape generates positive charges, while PET generates negative charges after the contact due to the electrification in triboelectric series.[20,25,26] Additionally, based on the electrostatic theory of adhesive, the contact between polymer adhesive materials and adherend generates a strong attractive force.[27] Since the adhesive bonding strength depends on the attractive force in the double layer, a higher charge generation can be achieved compared to the configuration using a non-tacky triboelectric layer in the existing TENGs. Since the PET layer is negatively charged, electrons in the Al layer on the PET will experience a repulsive force so that those electrons will flow to the ground. Therefore, a negative voltage occurs during the contact process, as shown in Figure 1c. In the separation process, the discharging behavior is quite different compared to the case in existing TENGs. Instead of the field-induced phenomenon as experienced in existing TENGs, an air breakdown induces a sudden electron removal in the PET layer. Such air breakdown causes neutralization of the PET layer so that electrons can flow back from the ground to the Al layer with positive charges, as shown in Figure 2b.[19,28−30] As a result, a positive voltage appears during the separation. From the electrostatic theory of adhesive, it is expected that the separation of adhesive will lose charges by field emission and gas ionization.[27] The actual electric spark generation was observed and will be discussed in the later part of this paper.

As shown in Figure 3a, the power is a function of the resistance load and driven frequency in the shaker test. It is very important to determine the frequency and resistance load effects on the performance of our triboelectric generator. A 4 MΩ resistance load yields the peak power under all frequencies, which corresponds to the impedance matching

https://doi.org/10.1021/acsomega.2c05457
ACS Omega 2022, 7, 42359−42369

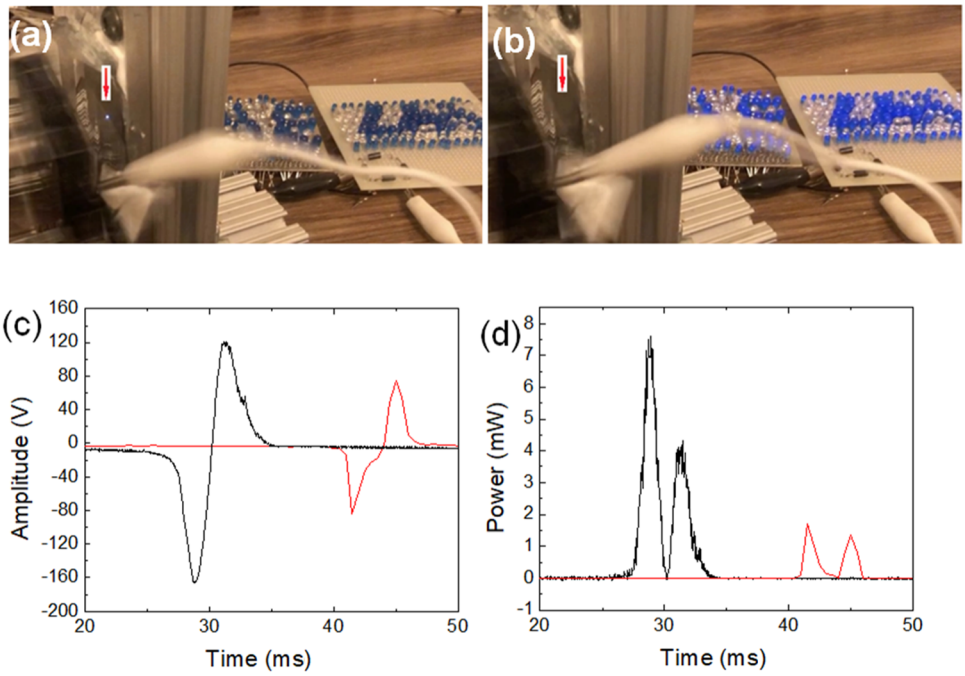

Figure 4. (a) Shaker operating triboelectric generator with Al/PET/tape−PET/Al combinations. During its operation, an electric spark occurs between the double-sided tape and PET/Al. This strongly indicates that the discharge between triboelectric layers occurs. (b) Within 33 ms after discharge (1 frame), the Al layer brings electrons from the ground because it still has the remaining positive charges. Therefore, lighting up of 296 LEDs is confirmed. (c) Comparison of voltage amplitude between double-sided tape−PET /Al(black) and double-sided tape−Al/PET configurations (red). Due to the Schottky barrier height for tape/Al interface, less electrons will overcome the barrier thermionically. (d) Consequently, power generation is significantly lower for double-sided tape−Al/PET combinations (red) compared to that for double-sided tape−PET/Al(black).

condition.[16,31] Also, the power generation shows frequency-dependent characteristics. A higher power value was observed around 20−22 Hz. As aforementioned, a load transducer was used to record the force during the impact. As shown in Figure 3b, the pressure was calculated using the measured force data under different driven frequencies. A higher pressure (force/unit area) value by the resonance frequency at 20−22 Hz corresponds to higher power generation, which indicates that a higher force generates charges more rapidly at a given time in the double layer during the contact phase. As a result, different frequencies with various pushing/pulling forces during a contact−separation process determine how fast electrical charges are generated through the system. Namely, if the contact and the separation processes occur with a faster impact, the electrical charge generation and dissipation occur abruptly, which results in having higher amplitudes.

To further understand the effect of triboelectric series on power generation, two configurations were evaluated, in which a double-sided tape is interfaced with either PET or Al side. Figure 4c shows the time history of collected voltage data, as plotted in black for the case with the interface between a double-sided tape and PET, and in red for the case with the interface between a double-sided tape and Al. The amount of power generation for both configurations is shown in Figure 4d. Higher peak power is observed in the case of the interface between a double-sided tape and PET due to the triboelectric series and Schottky effects. The triboelectric difference between a double-sided tape (i.e., acrylic adhesive layer) and a PET layer is higher than the case between a double-sided tape and an Al layer. When a double-sided tape layer is interfaced with an Al metal layer, electrons are created on the Al side during the contact phase. However, such electrons must overcome the Schottky barrier back and forth in a way of thermionic emission at the interface.[27,32] It is well known that the thermionic emission of metal will decrease the efficiency of triboelectric generators.[32] Since electrons are generated, an n-type Schottky barrier needs to be considered as it is defined as a product of the metal work function subtracted by the electron affinity of material at the interface. This strongly indicates that the electrostatic bonding nature between acrylic adhesive and Al is significantly less strong than the case with the interface between a double-sided tape and a PET sheet due to Schottky barrier formation at the metal interface.[27] It was also discussed that the negatively charged dielectric layer with higher work function (acrylic work function: 5.5 eV) than metal (Al work function: 4.2 eV) gives electrons to a metal after forming a contact and aligning the Fermi level.[21,33,34]

Knowing that PET made a better contact surface for the double-sided tape than aluminum, a double-electrode design was proposed to improve the performance of our triboelectric generator, as shown in Figure 5a, in which an additional PET/Al sheet is used to form a double-electrode configuration. Similar to the single-electrode design as shown in Figure 2a, we expect to utilize the electric charges on both sides of the double-sided tape during the contact and separation. Two separate electrical circuits were built to collect the voltage data separately. During the phase, the assembly on the right-hand side will generate positive charges in the tape layer and negative charges in the PET layer, as shown in Figure 5b. The Al electrode layer will flow electrons to the ground, as previously described in Figure 2b. No charge will be generated in the assembly on the left-hand side since the PET/Al layer was initially attached to the tape layer. Instead, the Al electrode layer on the left will bring electrons from the ground because

https://doi.org/10.1021/acsomega.2c05457
ACS Omega 2022, 7, 42359−42369

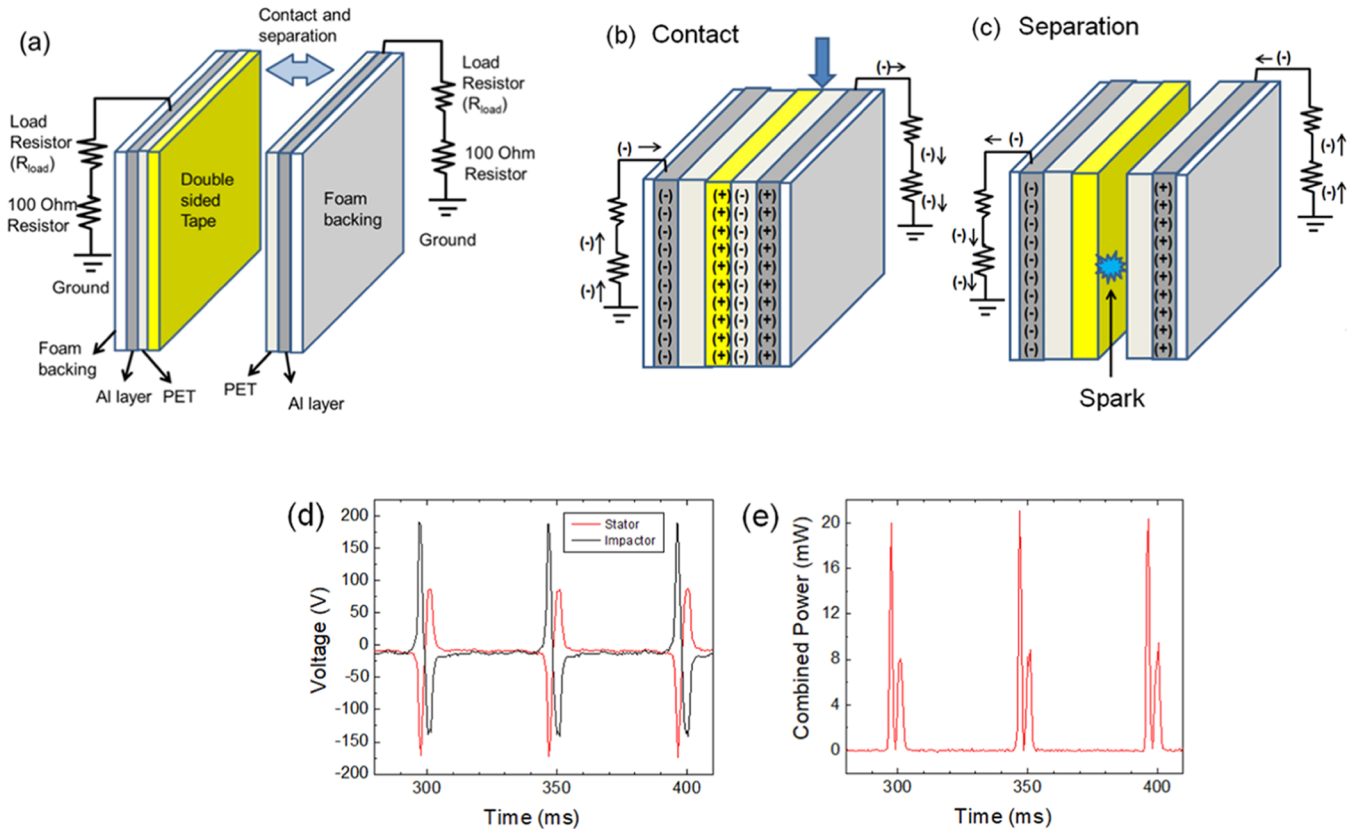

Figure 5. (a) Schematic of triboelectric generator with Al/PET/tape and PET/Al configurations. Separate electrical circuits are built for measuring voltage, current, and power on each side. (b) In the contact process, the electric double layer occurs at the interface between the double-sided tape and PET layer on the right side. Since PET on the left side was not used as a triboelectric layer, it was not charged up. Due to the positive charges in the double-sided tape, electrons will flow from the ground to Al layer. On the right side, with negatively charged PET, electrons will be pushed out from the Al layer to the ground. Therefore, the voltage amplitude signs on each side are opposite to each other. (c) In the separation process, the electrons are discharged in PET by the spark generation between the double-sided tape and PET on the right side. On the left Al layer, since the double-sided tape does not have any charges to attract electrons, electrons in the Al layer flow to the ground. On the right side, positive charges in Al will attract electrons from the ground. It shows similar behavior with contact process but with opposite signs of voltage amplitudes. (d) Amplitudes as a function of time for the left side Al layer (impactor—red) and right side Al layer (stator—black). As expected, amplitude signs are opposite for stator and impactor. (e) Corresponding power from combining the left and right sides. Peak power at 21.2 mW is obtained, which is significantly higher than that of a one-electrode Al layer configuration.

the tape was positively charged due to the contact. During the separation phase, electrons will flow from the ground in the Al electrode layer on the right since the negatively charged PET layer becomes neutral by sparking after the separation from the tape. The Al electrode layer on the left will bring electrons back to the ground since the charges on the tape were dissipated by sparking, as described in Figure 2b. Therefore, both Al electrode layers will have an opposite sign of voltage amplitude, as explained during the contact and separation motion. Figure 5d,e shows the voltage amplitude of the left Al layer (denoted as an impactor in red)/the right Al layer (denoted as a stator in black) and the combined power as a function of time, respectively, at 20 Hz. As expected, the voltage amplitude signs are exactly opposite on both sides. The combined power shows a peak value of 21.2 mW. The associated power density is calculated at 17.3 W/m^2, which is comparable to the value in existing TENGs. Furthermore, the efficiency of the system can be estimated by calculating both the input kinetic energy and output electrical energy.[35] The kinetic energy (KE) is given by

$$\mathrm{KE} = \frac{1}{2}mv^2 = \frac{1}{2} \times 0.1\ \mathrm{kg} \times \left(\frac{2\ \mathrm{mm}}{0.025\ \mathrm{s}}\right)^2 = 320\ \mu\mathrm{J}$$

Here, m is the mass of Al impactor. An average velocity (v) is assumed.

The output electrical energy is 27.4 μJ by integrating the power over time. Finally, the efficiency can be determined by taking the ratio between the input and output power, which is 8.6%.

A bridge rectifier circuit was used to convert AC voltage to DC voltage to demonstrate the direct power of 296 LEDs, which are connected in series as shown in Figure 6a during a shaker test with a driven frequency of 20 Hz. The voltage amplitude across 296 LEDs is up to 700 V, as shown in Figure 6b. Compared to the voltage data, a narrow-banded feature was observed in the power data, as shown in Figure 6c. The peak power has a value of 25 mW, i.e., 20.4 W/m^2 power density, which is able to power LEDs with high brightness, as shown in Figure 6d. The corresponding video footage is shown in S4.

Several manually operated triboelectric energy harvester prototypes were developed to further demonstrate the operation under low-frequency (i.e., < 5Hz) motion, in which a double-electrode configuration is adopted with an active area of 25 mm × 25 mm. As shown in Figure 7a, the pressing (contact) will generate a very strong restoring force by

https://doi.org/10.1021/acsomega.2c05457
ACS Omega 2022, 7, 42359−42369

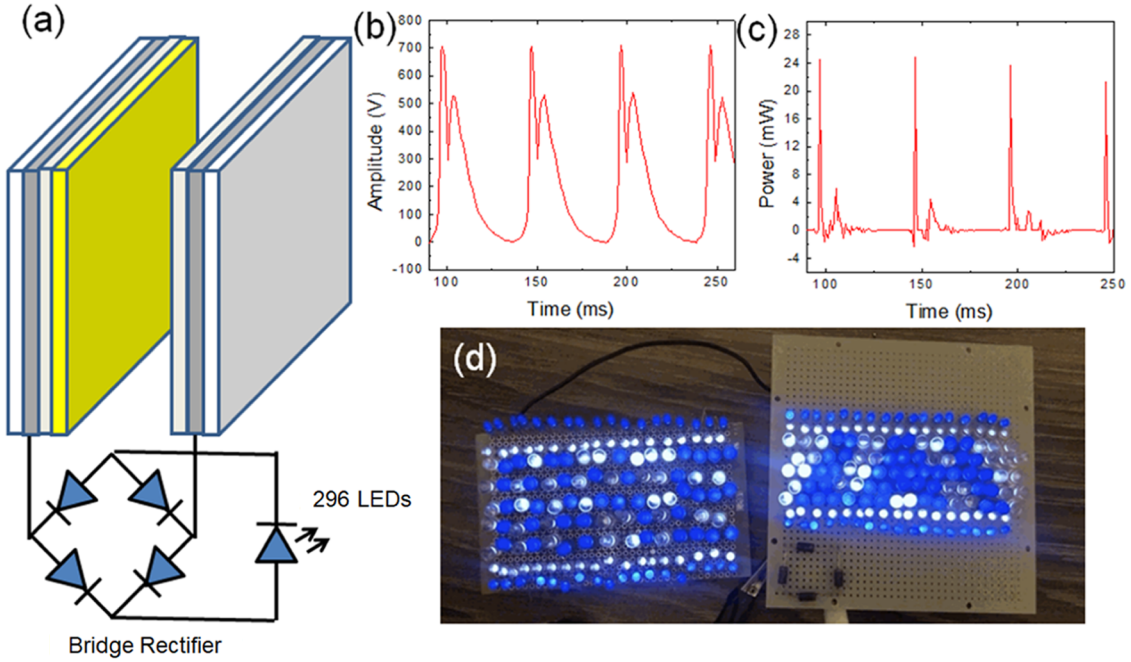

Figure 6. (a) Schematic of the triboelectric generator with Al/PET/tape−PET/Al combinations for DC pulse generation. A bridge rectifier was connected with the triboelectric generator and 296 LEDs in series. (b) DC voltage amplitude as a function of time for 296 LEDs. Negative amplitude generation becomes positive after passing the rectifier. (c) Corresponding power for 296 LEDs. A maximum power at 25 mW was generated during the process. (d) 296 LEDs light up during the triboelectric generator operation at 20 Hz.

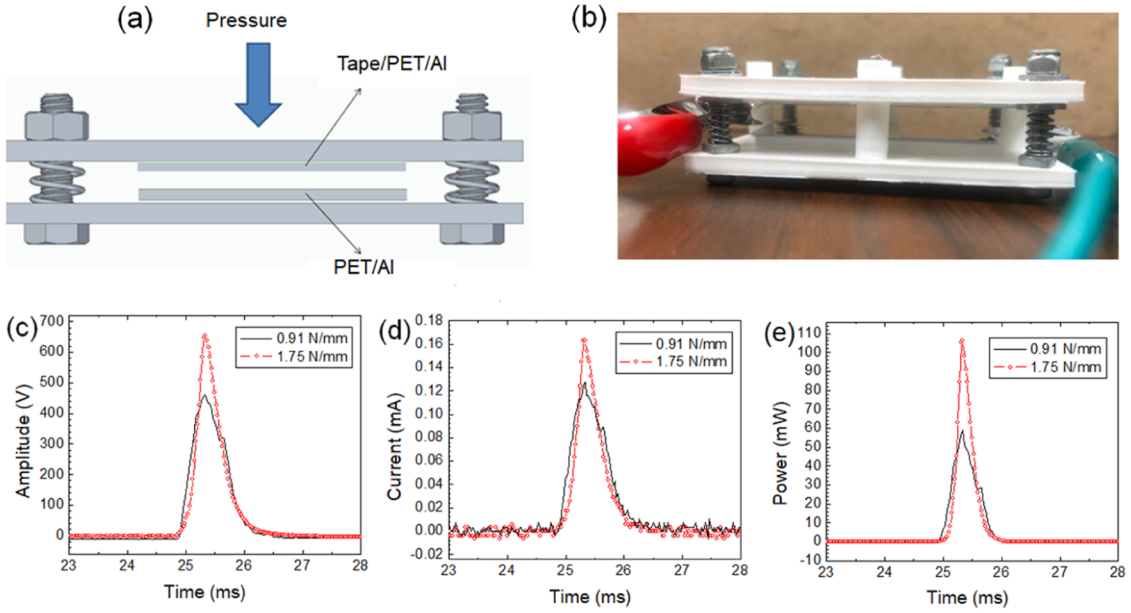

Figure 7. (a) Cross-sectional view of a manual triboelectric generator. Triboelectric layers are separated by four loaded springs at each corner. Once pressure is applied, triboelectric layers touch each other and are released quickly due to compressed springs. (b) 3D printed manual harvester with two electrical wires connecting both PET/Al layers to the circuit. (c) Voltage amplitude and (d) current data of the manual harvester with 0.91 and 1.75 N/mm spring constants, respectively. (e) Peak power generation for the manual harvester with 0.91 and 1.75 N/mm spring constants, respectively.

loaded springs during the separation process. Both soft spring and hard spring cases were investigated, which correspond to the spring constants at 0.91 N/mm and 1.75 N/mm, respectively, with four springs at each corner with a 10 mm gap between plates. A 4 MΩ load resistor and a 100 Ω resistor were introduced to collect voltage and current data during the manual press/release operation approximately at 1 Hz. As shown in Figure 7c−e, the voltage, current, and power responses show higher values when the spring constant is high. The highest peak power is 106 mW, and the associated power density (defined by power/unit area) is 169.6 W/m^2, which exceeds 47% to the highest value observed in existing TENGs.[19]

A second V-shaped triboelectric generator prototype was developed as well for a "hand castanets" operation, in which a folded polypropylene plate with a triboelectric assembly on

https://doi.org/10.1021/acsomega.2c05457
ACS Omega 2022, 7, 42359−42369

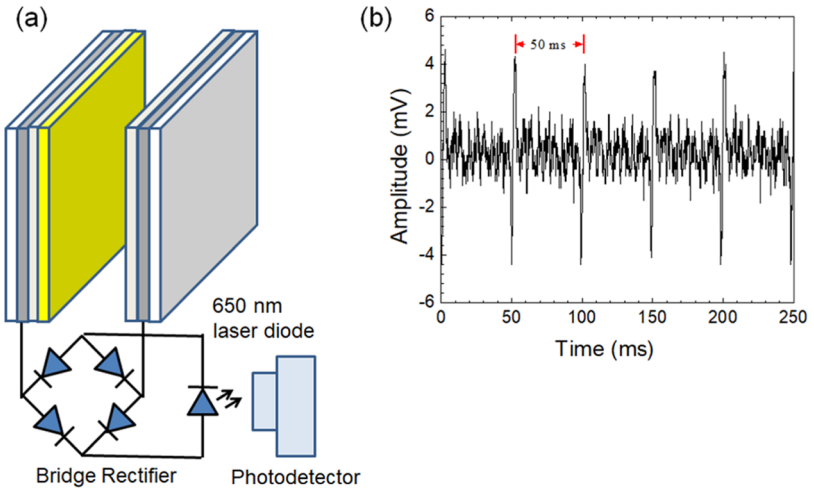

Figure 8. (a) Schematic of triboelectric generator with Al/PET/double-sided tape and PET/Al configuration for a DC pulse generation used for a lasing with a stimulus emission at 20 Hz of shaker frequency. (b) A stimulus emission of a 650 nm diode laser was confirmed with a 50 ms duration from a Si photodetector.

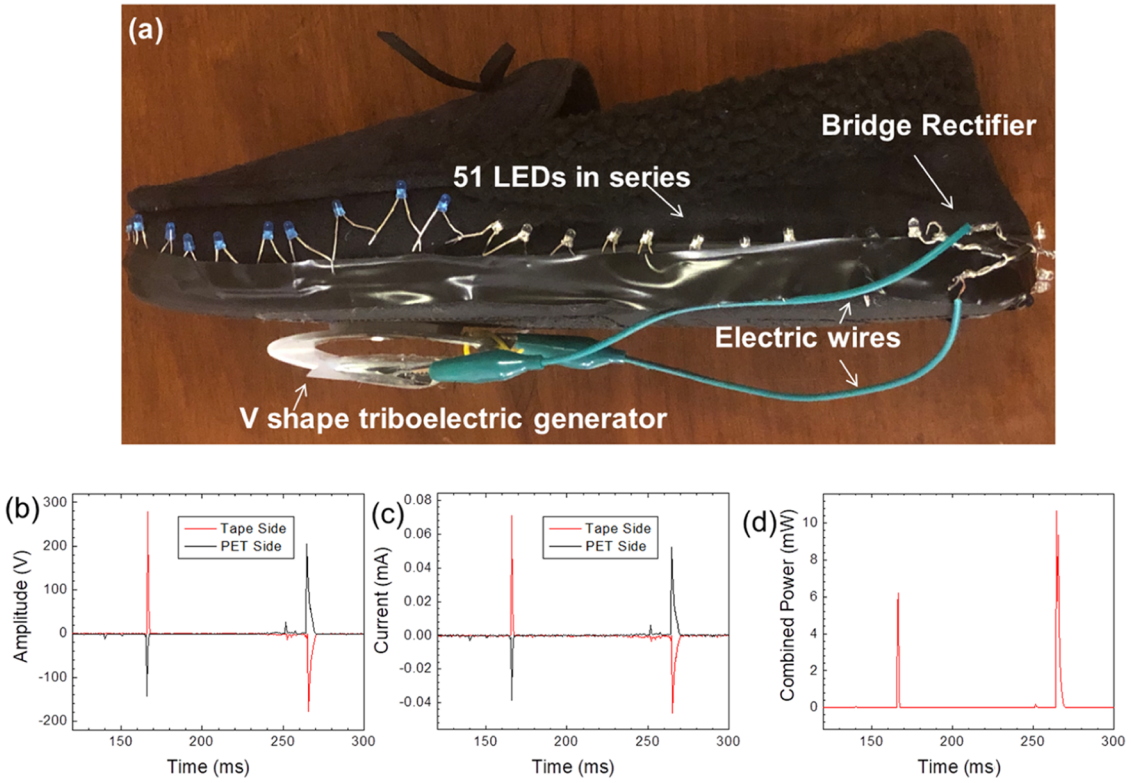

Figure 9. (a) Triboelectric generator (Al/PET/double-sided tape and PET/Al configuration) with a 38 mm × 38 mm area installed on the bottom of a shoe. A bridge rectifier circuit is used to convert AC to DC power to demonstrate the lighting up of 51 LEDs; (b) voltage; (c) current; and (d) power under a 4 MΩ electrical load.

each inner surface is employed. This manual triboelectric generator lights up 476 LEDs operated approximately at 2 Hz, which has a 38 mm by 25 mm active area. Associated videos are shown in S5 and S6. Additional 20 more LEDs were lit compared to that in a typical TENG device.[19]

A 650 nm laser diode was powered using our double-electrode triboelectric generation under a shaker test, as shown in Figure 8a. Videos of power LEDs and a laser diode in a two-in-one flashlight are shown in S7 and S8, respectively. Figure 8b shows a photodetector amplitude signal of the laser diode as a function of time. Clearly, the overcoming of the lasing threshold is observed from the laser diode with an indication of the stimulus emission for the first time in the triboelectric generator. In addition, the laser operation shows a 50 ms interval, which corresponds to the driven frequency of 20 Hz in the shaker test.

A V-shaped manual triboelectric generator with a 38 mm × 38 mm active area assembled as the Al/PET/double-sided tape and PET/Al was inserted at the bottom of a shoe, as shown in Figure 9a, to demonstrate energy harvesting via walking. A bridge circuit and 51 LEDs are connected to convert the AC electric signals into DC for lighting up LEDs. The amount of

https://doi.org/10.1021/acsomega.2c05457
ACS Omega 2022, 7, 42359−42369

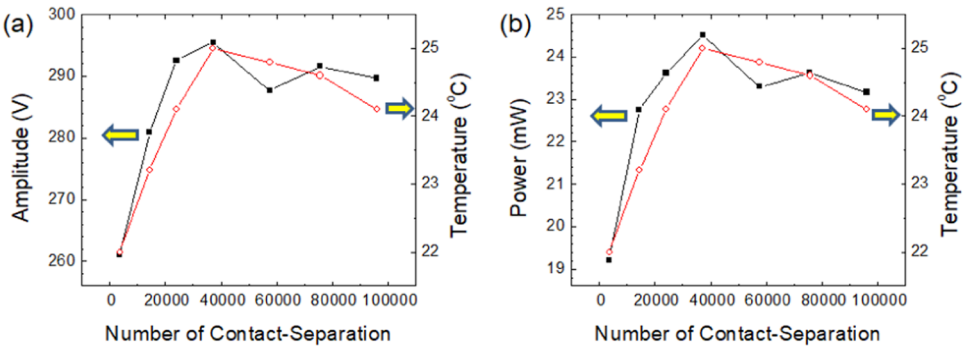

Figure 10. (a) Voltage amplitude for a triboelectric generator with a double-electrode configuration in a shaker test to reach 100,000 contact−separation cycles. Temperature data in red were collected at the Al framing (shown in Figure 1). (b) Corresponding peak power under a 4 MΩ electrical load

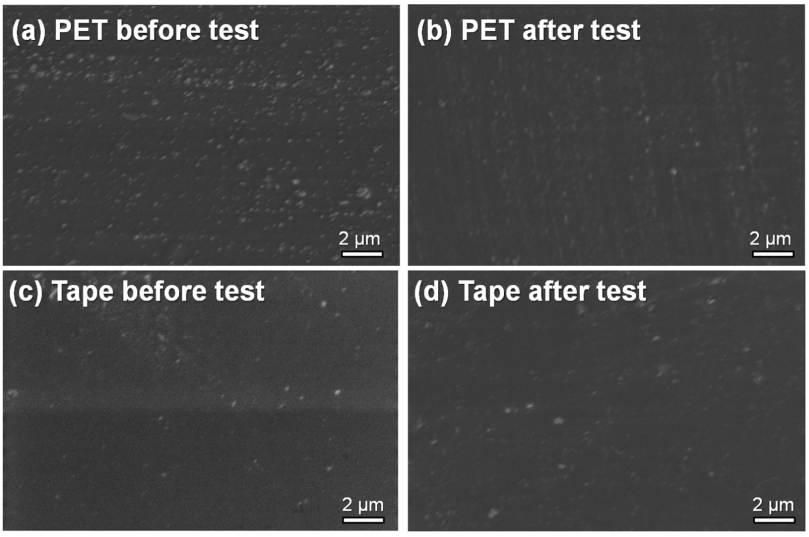

Figure 11. SEM images of PET (a) before and (b) after endurance test and double-sided tape (c) before and (d) after endurance test at 20,000× magnification.

peak power generation was confirmed, as shown in Figure 9b−d. It shows that the peak power is over 10 mW, which indicates that the double-sided tape triboelectric generator can be easily adapted to real-world applications without any issues at low-frequency ranges. A video for this demonstration is shown in S9.

Figure 10 shows the endurance test results for a triboelectric generator with a double-electrode configuration, in which an electrical load of a 4 MΩ resistor is connected. Both voltage and temperature data were recorded up to 100,000 contact−separation cycles. Since the temperature increases gradually, the voltage amplitude increases accordingly. Clearly, the temperature has an effect on the performance of power generation because more charges will be transmitted between insulating triboelectric layers.[32] After 40,000 contact−separation events, the temperature decreases gradually so that the performance degrades slightly. Comparable power generation is achieved up to 100,000 cycles, which varies from 19 to 24 mW.

Figure 11 shows SEM images of both tape and PET surfaces before and after the test. Before the test, the PET shows many particles on its surface due to the electrostatic attraction. After the test, less particles are observed. There is no major morphological change in the double-sided tape. This indicates that there is no substantial degradation in adhesiveness.

CONCLUSIONS

In this paper, a simple triboelectric generator concept was proposed, evaluated, and demonstrated, which is composed of a double-sided tape and a PET/Al sheet. Power generation is comparable with the current state of the art of TENG devices. Key conclusions are summarized below:

- This is the first attempt to use tacky materials in the triboelectric generator.
- This novel double-sided tape triboelectric generator shows the potential to improve the performance of energy harvesting via triboelectrification.
- Such a simple design leads to easy fabrication and integration, which only requires a craft-level skill compared to the nanotechnology-based sophisticated fabrication scheme used in current TENGs.
- In polymer-based adhesives, the bonding strength depends on the electrical double layer at the interface with positive and negative charges on each side.
- The strong bonding nature of acrylic adhesive in a double-sided tape induces a significant charge when contacting the PET layer.
- Air breakdown between triboelectric layers occurs during the separation phase to enable rapid charge

https://doi.org/10.1021/acsomega.2c05457
ACS Omega 2022, 7, 42359−42369

removal, which actually helps electrons to flow much easier.

- The first attempt to power a 650 nm laser diode using our TENG, which is crucial for optoelectronic devices and sensor applications.

■ ASSOCIATED CONTENT

Supporting Information

The Supporting Information is available free of charge at https://pubs.acs.org/doi/10.1021/acsomega.2c05457.

FTIR absorbance spectrum for a double-sided tape (Figure S1); voltage amplitude of a triboelectric generator with a 1 MΩ resistor in a shaker test (Figure S2) (PDF)

Video to show a triboelectric generator (Al/PET/double-sided tape−PET/Al configuration) under a shaker test at 20 Hz; an electric spark generation is confirmed between triboelectric layers (S3a) (MP4)

Video to show a manual triboelectic generator (Al/PET/double-sided tape−PET/Al configuration); electric spark generation is confirmed near electrodes (S3b) (MP4)

Video to show a direct power of 296 LEDs using a triboelectric generator (Al/PET/double-sided tape−PET/Al) driven by a shaker at 20 Hz; electrical wires from the triboelectric generator were connected to a bridge rectifier to provide DC power (S4) (MP4)

Video to show direct power 476 LEDs using a V-shaped manual triboelectric generator (Al/PET/double-sided tape−PET/Al configuration) (S5) (MP4)

Video at a slow speed (12.5% from the normal speed) to show direct power 476 LEDs using a V-shaped manual triboelectric generator (Al/PET/double-sided tape−PET/Al configuration) (S6) (MP4)

Video to show a direct power of a flashlight using a triboelectric generator (Al/PET/double-sided tape−PET/Al configuration) driven by a shaker at 20 Hz (S7) (MP4)

Video to show a direct power of a 650 nm diode laser using a triboelectric generator (Al/PET/double-sided tape−PET/Al configuration) driven by a shaker at 20 Hz (S8) (MP4)

Video to show a direct power of 51 LEDs while stepping using a triboelectric generator, as shown in Figure 9 (S9) (MP4)

■ AUTHOR INFORMATION

Corresponding Author

Gang Wang − *Department of Mechanical and Aerospace Engineering, The University of Alabama in Huntsville, Huntsville, Alabama 35899, United States;* orcid.org/0000-0001-9843-5966; Email: gang.wang@uah.edu

Authors

Moon-Hyung Jang − *Department of Mechanical and Aerospace Engineering, The University of Alabama in Huntsville, Huntsville, Alabama 35899, United States; Department of Chemical and Materials Engineering, The University of Alabama in Huntsville, Huntsville, Alabama 35899, United States*

Jacob D. Lee − *Department of Mechanical and Aerospace Engineering, The University of Alabama in Huntsville, Huntsville, Alabama 35899, United States*

Yu Lei − *Department of Chemical and Materials Engineering, The University of Alabama in Huntsville, Huntsville, Alabama 35899, United States;* orcid.org/0000-0002-4161-5568

Simon Chung − *Materials Sciences LLC, Horsham, Pennsylvania 19044, United States*

Complete contact information is available at: https://pubs.acs.org/10.1021/acsomega.2c05457

Author Contributions

G.W. proposed the idea of using an Al/PET sheet as a triboelectric layer. M.-H.J. proposed the idea of using a double-sided tape as another triboelectric layer. Shaker and manual triboelectric generator tests were performed by M.-H.J. Manual generator design was proposed by J.D.L. M.-H.J. analyzed the data. Results are discussed by M.-H.J., G.W., J.D.L., Y.L., and S.C. M.-H.J., G.W., and J.D.L. prepared the manuscript.

Notes

The authors declare no competing financial interest.

■ ACKNOWLEDGMENTS

This project was partially supported by the College of Engineering at the University of Alabama in Huntsville and Material Sciences LLC.

■ REFERENCES

(1) Geim, A. K. Nobel Lecture: Random walk to graphene. *Rev. Mod. Phys.* **2011**, *83*, 851−862.

(2) Camara, C. G.; Escobar, J. V.; Hird, J. R.; Putterman, S. J. Correlation between nanosecond X-ray flashes and stick−slip friction in peeling tape. *Nature* **2008**, *455*, 1089−1092.

(3) Luo, J.; Wang, Z. L. Recent progress of triboelectric nanogenerators: From fundamental theory to practical applications. *EcoMat* **2020**, *2*, No. e12059. (acccessed 2021/06/24).

(4) Dong, K.; Wu, Z.; Deng, J.; Wang, A. C.; Zou, H.; Chen, C.; Hu, D.; Gu, B.; Sun, B.; Wang, Z. L. A Stretchable Yarn Embedded Triboelectric Nanogenerator as Electronic Skin for Biomechanical Energy Harvesting and Multifunctional Pressure Sensing. *Adv. Mater.* **2018**, *30*, No. 1804944. (acccessed 2021/06/24).

(5) Tang, Q.; Yeh, M.-H.; Liu, G.; Li, S.; Chen, J.; Bai, Y.; Feng, L.; Lai, M.; Ho, K.-C.; Guo, H.; Hu, C. Whirligig-inspired triboelectric nanogenerator with ultrahigh specific output as reliable portable instant power supply for personal health monitoring devices. *Nano Energy* **2018**, *47*, 74−80.

(6) Li, Z.; Feng, H.; Zheng, Q.; Li, H.; Zhao, C.; Ouyang, H.; Noreen, S.; Yu, M.; Su, F.; Liu, R.; et al. Photothermally tunable biodegradation of implantable triboelectric nanogenerators for tissue repairing. *Nano Energy* **2018**, *54*, 390−399.

(7) Liu, Z.; Li, H.; Shi, B.; Fan, Y.; Wang, Z. L.; Li, Z. Wearable and Implantable Triboelectric Nanogenerators. *Adv. Funct. Mater.* **2019**, *29*, No. 1808820. (acccessed 2021/06/24).

(8) Huang, C.; Chen, G.; Nashalian, A.; Chen, J. Advances in self-powered chemical sensing via a triboelectric nanogenerator. *Nanoscale* **2021**, *13*, 2065−2081.

(9) Wang, Z. L.; Wu, W. Nanotechnology-Enabled Energy Harvesting for Self-Powered Micro-/Nanosystems. *Angew. Chem., Int. Ed.* **2012**, *51*, 11700−11721. (acccessed 2021/06/24).

(10) Su, Y.; Li, W.; Yuan, L.; Chen, C.; Pan, H.; Xie, G.; Conta, G.; Ferrier, S.; Zhao, X.; Chen, G.; et al. Piezoelectric fiber composites with polydopamine interfacial layer for self-powered wearable biomonitoring. *Nano Energy* **2021**, *89*, No. 106321.

(11) Li, W.; Yang, T.; Liu, C.; Huang, Y.; Chen, C.; Pan, H.; Xie, G.; Tai, H.; Jiang, Y.; Wu, Y.; et al. Optimizing Piezoelectric Nanocomposites by High-Throughput Phase-Field Simulation and Machine Learning. *Adv. Sci.* **2022**, *9*, No. 2105550.
(12) Su, Y.; Li, W.; Cheng, X.; Zhou, Y.; Yang, S.; Zhang, X.; Chen, C.; Yang, T.; Pan, H.; Xie, G.; et al. High-performance piezoelectric composites via β phase programming. *Nat. Commun.* **2022**, *13*, No. 4867.
(13) Wang, Z. L. L.; Chen, Jun.; Niu, S.; Zi, Y.*Triboelectric Nanogenerators*; Springer International Publishing, 2016.
(14) Su, Y.; Chen, G.; Chen, C.; Gong, Q.; Xie, G.; Yao, M.; Tai, H.; Jiang, Y.; Chen, J. Self-Powered Respiration Monitoring Enabled By a Triboelectric Nanogenerator. *Adv. Mater.* **2021**, *33*, No. 2101262.
(15) Wang, Y.; Yang, Y.; Wang, Z. L. Triboelectric nanogenerators as flexible power sources. *npj Flex. Electron.* **2017**, *1*, No. 10.
(16) Liu, W.; Wang, Z.; Wang, G.; Liu, G.; Chen, J.; Pu, X.; Xi, Y.; Wang, X.; Guo, H.; Hu, C.; Wang, Z. L. Integrated charge excitation triboelectric nanogenerator. *Nat. Commun.* **2019**, *10*, No. 1426.
(17) Wang, S.; Lin, L.; Xie, Y.; Jing, Q.; Niu, S.; Wang, Z. L. Sliding-Triboelectric Nanogenerators Based on In-Plane Charge-Separation Mechanism. *Nano Lett.* **2013**, *13*, 2226−2233.
(18) Li, Y.; Zhao, Z.; Liu, L.; Zhou, L.; Liu, D.; Li, S.; Chen, S.; Dai, Y.; Wang, J.; Wang, Z. L. Improved Output Performance of Triboelectric Nanogenerator by Fast Accumulation Process of Surface Charges. *Adv. Energy Mater.* **2021**, *11*, No. 2100050. (acccessed 2021/06/24).
(19) Liu, Y.; Liu, W.; Wang, Z.; He, W.; Tang, Q.; Xi, Y.; Wang, X.; Guo, H.; Hu, C. Quantifying contact status and the air-breakdown model of charge-excitation triboelectric nanogenerators to maximize charge density. *Nat. Commun.* **2020**, *11*, No. 1599.
(20) Zou, H.; Zhang, Y.; Guo, L.; Wang, P.; He, X.; Dai, G.; Zheng, H.; Chen, C.; Wang, A. C.; Xu, C.; Wang, Z. L. Quantifying the triboelectric series. *Nat. Commun.* **2019**, *10*, No. 1427.
(21) Zou, H.; Guo, L.; Xue, H.; Zhang, Y.; Shen, X.; Liu, X.; Wang, P.; He, X.; Dai, G.; Jiang, P.; et al. Quantifying and understanding the triboelectric series of inorganic non-metallic materials. *Nat. Commun.* **2020**, *11*, No. 2093.
(22) Han, M.; Z, X.; Zhang, H.*Flexible and Stretchable Triboelectric Nanogenerator Devices: Toward Self-powered Systems*; Wiley-VCH, 2019.
(23) Zięba-Palus, J. The usefulness of infrared spectroscopy in examinations of adhesive tapes for forensic purposes. *J. Forensic Sci. Criminol.* **2017**, *2*, 1−9.
(24) Zhu, G.; Pan, C.; Guo, W.; Chen, C.-Y.; Zhou, Y.; Yu, R.; Wang, Z. L. Triboelectric-Generator-Driven Pulse Electrodeposition for Micropatterning. *Nano Lett.* **2012**, *12*, 4960−4965.
(25) Wang, Z. L. From contact electrification to triboelectric nanogenerators. *Rep. Prog. Phys.* **2021**, *84*, No. 096502.
(26) Stranneby, D. ESD risks in industrial environments. *Electronic environment* **2013**, 10−13. Editorial material. (acccessed 2014-12-29t01:26:02.669+01:00).DiVA.
(27) Derjaguin, B. V.; Smilga, V. P. Electronic Theory of Adhesion. *J. Appl. Phys.* **1967**, *38*, 4609−4616. (acccessed 2021/11/18).
(28) Liu, D.; Zhou, L.; Li, S.; Zhao, Z.; Yin, X.; Yi, Z.; Zhang, C.; Li, X.; Wang, J.; Wang, Z. L. Hugely Enhanced Output Power of Direct-Current Triboelectric Nanogenerators by Using Electrostatic Breakdown Effect. *Adv. Mater. Technol.* **2020**, *5*, No. 2000289. (acccessed 2021/12/11).
(29) Cao, Z.; Chu, Y.; Wang, S.; Wu, Z.; Ding, R.; Ye, X. In *A Strategy to Reduce Air Breakdown Effect and Boost Output Energy for Contact-Separation Mode Triboelectric Nanogenerator*, In 2021 21st International Conference on Solid-State Sensors, Actuators and Microsystems (Transducers); IEEE, 20−24 June, 2021; pp 451−454, DOI: 10.1109/Transducers50396.2021.9495462.
(30) Zhou, L.; Liu, D.; Zhao, Z.; Li, S.; Liu, Y.; Liu, L.; Gao, Y.; Wang, Z. L.; Wang, J. Simultaneously Enhancing Power Density and Durability of Sliding-Mode Triboelectric Nanogenerator via Interface Liquid Lubrication. *Adv. Energy Mater.* **2020**, *10*, No. 2002920. (acccessed 2021/12/12).
(31) Quan, Z.; Han, C. B.; Jiang, T.; Wang, Z. L. Robust Thin Films-Based Triboelectric Nanogenerator Arrays for Harvesting Bidirectional Wind Energy. *Adv. Energy Mater.* **2016**, *6*, No. 1501799. (acccessed 2021/11/19).
(32) Xu, C.; Wang, A. C.; Zou, H.; Zhang, B.; Zhang, C.; Zi, Y.; Pan, L.; Wang, P.; Feng, P.; Lin, Z.; Wang, Z. L. Raising the Working Temperature of a Triboelectric Nanogenerator by Quenching Down Electron Thermionic Emission in Contact-Electrification. *Adv. Mater.* **2018**, *30*, No. 1803968. (acccessed 2022/06/07).
(33) Bai, P.; Zhu, G.; Zhou, Y. S.; Wang, S.; Ma, J.; Zhang, G.; Wang, Z. L. Dipole-moment-induced effect on contact electrification for triboelectric nanogenerators. *Nano Res.* **2014**, *7*, 990−997.
(34) Trigwell, S.; Grable, N.; Yurteri, C. U.; Sharma, R.; Mazumder, M. K. Effects of surface properties on the tribocharging characteristics of polymer powder as applied to industrial processes. *IEEE Trans. Ind. Appl.* **2003**, *39*, 79−86.
(35) Chun, J.; Ye, B. U.; Lee, J. W.; Choi, D.; Kang, C.-Y.; Kim, S.-W.; Wang, Z. L.; Baik, J. M. Boosted output performance of triboelectric nanogenerator via electric double layer effect. *Nat. Commun.* **2016**, *7*, No. 12985.

https://doi.org/10.1021/acsomega.2c05457
ACS Omega 2022, 7, 42359−42369